J. Phys. Chem. B **2007,** *111,* 12865−12875

An Improved Picture of Methyl Dynamics in Proteins from Slowly Relaxing Local Structure Analysis of ^{2}H Spin Relaxation

Eva Meirovitch,*,† Yury E. Shapiro,† Antonino Polimeno,*,‡ and Jack H. Freed*,§

The Mina and Everard Goodman Faculty of Life Sciences, Bar-Ilan University, Ramat-Gan 52900 Israel, Department of Physical Chemistry, University of Padua, 35131 Padua, Italy, and Baker Laboratory of Chemistry and Chemical Biology, Cornell University, Ithaca, New York 14853-1301

Received: March 18, 2007; In Final Form: July 30, 2007

Protein dynamics is intimately related to biological function. Core dynamics is usually studied with ^{2}H spin relaxation of the ^{13}CDH$_2$ group, analyzed traditionally with the model-free (MF) approach. We showed recently that MF is oversimplified in several respects. This includes the assumption that the local motion of the dynamic probe and the global motion of the protein are decoupled, the local geometry is simple, and the local ordering is axially symmetric. Because of these simplifications MF has yielded a puzzling picture where the methyl rotation axis is moving rapidly with amplitudes ranging from nearly complete disorder to nearly complete order in tightly packed protein cores. Our conclusions emerged from applying to methyl dynamics in proteins the slowly relaxing local structure (SRLS) approach of Polimeno and Freed (Polimeno, A.; Freed, J. H. *J. Phys. Chem.* **1995**, *99*, 10995−11006.), which can be considered the generalization of MF, with all the simplifications mentioned above removed. The SRLS picture derived here for the B1 immunoglobulin binding domain of peptostreptococcal protein L, studied over the temperature range of 15−45 °C, is fundamentally different from the MF picture. Thus, methyl dynamics is characterized structurally by rhombic local potentials with varying symmetries and dynamically by tenfold slower rates of local motion. On average, potential rhombicity decreases, mode-coupling increases, and the rate of local motion increases with increasing temperature. The average activation energy for local motion is 2.0 ± 0.2 kcal/mol. Mode-coupling affects the analysis even at 15 °C. The accuracy of the results is improved by including in the experimental data set relaxation rates associated with rank 2 coherences.

I. Introduction

NMR spin relaxation is a powerful method for studying protein dynamics.[1−9] The traditional probe for investigating backbone motion is the ^{15}N−^{1}H bond and the common probe for studying side chain motion is the uniformly ^{13}C-labeled and fractionally deuterated methyl group, ^{13}CH$_2$D.[5,6,10−12] In this study we focus on the latter. Methyl dynamics in proteins is analyzed typically with the model-free (MF) approach,[13−15] that assumes that the global and local motions of the probe are decoupled due to the former being much slower than the latter. This is an approximation, and so are the high symmetries assigned implicitly to the diffusion, ordering and magnetic tensors involved, and the coincidence of their frames, which simplifies the local geometry. By virtue of these simplifications, an analytical formula is obtained for the measurable spectral density,[13] specific values of which enter the expressions for the experimental relaxation rates. The original MF spectral density[13] is determined by an effective correlation time for local motion, τ_e, a squared generalized order parameter, S^2, representing the spatial restrictions at the site of the motion of the probe, and the global motion correlation time, τ_m. The latter is usually determined independently.

For methyl dynamics, MF considers two local motions including rotation *about* the C−CH$_3$ axis and fluctuations *of* the C−CH$_3$ axis.[10] Moreover, the methyl rotation axis C−CH$_3$ (to be denoted M$_z$, with M representing the local ordering/local diffusion frame) is tilted at $\beta_{MQ} = 110.5°$ from the magnetic quadrupolar frame, Q, which lies along the C−D bond (110.5° is the tetrahedral angle taking $r_{CH} = r_{CD} = 1.115$ Å).[12] Yet, as pointed out above, the original MF formula,[13] typically used in methyl dynamics analyses, features only one mode of local motion and has no provision for a “diffusion tilt”. These features entail further approximations (see below).

We have shown recently that the MF approach is oversimplified.[16−23] This has been accomplished by applying to NMR spin relaxation in proteins,[16] the slowly relaxing local structure (SRLS) approach of Freed and co-workers.[24−26] SRLS can be considered the generalization of MF, yielding the latter in asymptotic limits.[16,20,21,24] Unlike MF, the SRLS model takes into account rigorously the dynamical coupling between the global motion of the protein and the local motion of the dynamic probe, brought into effect by a rhombic coupling potential. It features explicitly local motional modes parallel and perpendicular to the local diffusion axis[16−23,25,26] and accounts rigorously for the tilt between a rhombic local ordering frame, M, and the magnetic frame, Q. The Euler angles $\Omega_{C'M}$, which relate the M frame to a local director frame, C′ (e.g., the equilibrium C−CH$_3$ orientation), are associated with the coupling/ordering potential. In general “dynamical coupling” means that through the time dependence of $\Omega_{C'M}$, the locally reorienting dynamic probe follows the slower motion of the protein. In the limit where the time scale separation between the global and local motions is large this concept is associated primarily with local motional mode multiplicity.

---

* Corresponding authors. E-mail: eva@nmrsgi5.ls.biu.ac.il (E.M.); jhf@ccmr.cornell.edu (J.H.F.); antonino.polimeno@unipd.it (A.P.).

† Bar-Ilan University.

‡ University of Padua.

§ Cornell University.

10.1021/jp072156s CCC: $37.00

The MF simplifications have far-fetched implications. For a M frame tilted relative to the Q frame, the spectral density, $J^{QQ}(\omega)$ (QQ denotes quadrupolar auto-correlated relaxation), comprises three generic spectral density functions, $j_K(\omega)$, with $K = 0, 1, 2$, by analogy with $J(\omega)$ for axial global diffusion of a rigid protein comprising three Lorentzian functions with $K = 0, 1, 2$. Yet, the MF spectral density consists of a single function which represents the $K = 0$ contribution. Various parametrizations of its form have been attempted to overcome the flaw of omission of the $K = 1$ and $K = 2$ contributions. If the local ordering frame, M, is rhombic, as we found it to be,[23] cross-term functions $j_{KK'}(\omega)$ will also enter the expression for $J^{QQ}(\omega)$. This renders the parametrized MF spectral density to be very different from the actual spectral density. However, in many cases the experimental data can be reproduced by force-fitting, with the statistical criteria fulfilled, but the best-fit parameters (S^2 and τ_e) highly inaccurate.[23]

The form of $J^{QQ}(\omega)$ is parametrized in MF as follows. To accommodate two local motional modes, S^2 is factored into the product $[P_2(\cos 110.5°)]^2 \times S_{\mathrm{axis}}{}^2 = 0.1 S_{\mathrm{axis}}{}^2$. The term $[P_2(\cos 110.5°)]^2 = 0.1$ represents the squared order parameter for methyl rotation *about* C$-$CH$_3$ (ref 27a), and $S_{\mathrm{axis}}{}^2$ the *axial* squared order parameter for motion *of* the C$-$CH$_3$ axis.[10,27b] As outlined below in detail, factoring S^2 as shown, with the meaning of the constituents as indicated, is only valid when τ_e is in the extreme motional narrowing limit.[23,27c,d] Yet, in practice finite values of τ_e are required in MF analyses to fit the experimental data.

Practical implications of the MF simplifications have been investigated recently[23] using the B1 immunoglobulin binding domain of peptostreptococcal protein L (to be called "protein L" from this point)[12] and ubiquitin[28] as test cases. The respective data were subjected to SRLS analysis,[23] and the emerging dynamic pictures were compared with the corresponding previously obtained MF pictures.[12,28]

We found that rhombic local potential/local ordering is required to analyze methyl dynamics consistently and insightfully.[23] MF analyses yield unduly large distributions in the value of $S_{\mathrm{axis}}{}^2$ ranging from nearly complete disorder ($S_{\mathrm{axis}}{}^2 \sim 0.1$) to nearly complete order ($S_{\mathrm{axis}}{}^2 \sim 1$), often exhibiting three distinct maxima.[6,28-31] The (pervasive) low $S_{\mathrm{axis}}{}^2$ values imply large-amplitude excursions of the C$-$CH$_3$ axis in tightly packed protein cores.[6] Interpretation in terms of limited excursions using the 1D and 3D Gaussian axial fluctuations (GAF) models[32-34] is incompatible with axial symmetry around the C$-$CH$_3$ axis, inherent in the definition of $S_{\mathrm{axis}}{}^2$ (ref 27b). Contrary to the problematic MF picture, SRLS interprets the variations in the experimental data as variations in the symmetry, and to some extent the magnitude, of the local ordering potential (or local ordering tensor).[23] The three categories of $S_{\mathrm{axis}}{}^2$ values correspond to different forms (symmetries) of the rhombic local potential.[23] This is physically tenable, provides new and interesting site-specific structural information, and agrees with NMR *J*-coupling and reduced dipolar coupling,[35,36] molecular-dynamics (MD)[37,38] and molecular mechanics[39] studies. All of these investigations have shown that local structural asymmetry prevails at methyl sites in proteins, contrary to the axial $S_{\mathrm{axis}}{}^2$ based MF picture.

The present paper is an extension of our previous study[23] which was based on ^{2}H T_1 and T_2 data acquired for protein L[12] and ubiquitin[28] at ambient temperature and magnetic fields of 11.7 and 14.1 T. Kay and co-workers developed pulse sequences for measuring relaxation rates associated with double-quantum, two-spin-order and antiphase rank 2 coherences,[11] in addition to ^{2}H T_1 and T_2.[10] For protein L, the Kay group acquired all five ^{2}H relaxation rates at 5, 15, 25, 35, and 45 °C at a magnetic field of 11.7 T. At 25 (5) °C additional data were acquired at magnetic fields of 9.4, 14.1, and 18.8 (14.1) T. This is among the most extensive and robust data sets of autocorrelated ^{2}H relaxation rates currently available. In the present study we used these data, kindly provided by Prof. L. E. Kay, to explore temperature, magnetic field, and rank 2 coherence dependence and treat several important aspects of methyl dynamics. The issue of relatively large uncertainties in the best-fit parameters, implied by the relatively narrow portion of $J^{QQ}(\omega)$ sampled by the experimental data, is addressed. Note that unlike the case of proton-bound heteronuclei, where ^{1}H contributes high-frequency $J(\omega)$ values through the NOE, for ^{2}H relaxation only the $\omega = 0$, ω_D, and $2\omega_D$ values, with ω_D denoting the ^{2}H resonance frequency, are sampled at any given magnetic field. In this context, the benefit of using up to four-field data sets, including rank 2 coherences, is explored herein.

We find that the protein L methyl sites exhibit rhombic potentials of different forms in the SRLS scenario instead of amplitudes of C$-$CH$_3$ motion of different extents in the MF scenario. The local motional modes are 10-fold slower in the SRLS scenario. Mode-coupling is important even at 15 °C. On average, potential rhombicity decreases, mode-coupling increases, and the rate of local motion increases with increasing temperature. The average activation energy for local motion is 2.0 ± 0.2 kcal/mol. The accuracy of the results is improved by including in the experimental data set relaxation rates associated with rank 2 coherences.

The theoretical background appears in section II. The various topics mentioned above are treated under Results and Discussion in section III. Our conclusions appear in section IV.

II. Theoretical Background

The Theoretical Background relevant for this paper appears in ref 23. For convenience a brief summary is presented below.

1. The Model-Free (MF) Approach. The original MF spectral density, $J(\omega)$, based on $\tau_e \ll \tau_m$ (i.e., an effective local motion, τ_e, much faster than the global motion, τ_m), is given by[13]

$$J(\omega) = S^2\tau_m/(1 + \tau_m{}^2\omega^2) + (1 - S^2)\,\tau_e{}'/(1 + \tau_e{}'^2\omega^2) \quad (1)$$

where $1/\tau_e{}' = 1/\tau_m + 1/\tau_e \sim 1/\tau_e$.

This equation has been adapted to methyl dynamics where two restricted local motions *about* and *of* the methyl averaging axis are considered[10,27a] by setting S^2 equal to $[P_2(\cos 110.5°)]^2 \times S_{\mathrm{axis}}{}^2 = 0.1 \times S_{\mathrm{axis}}{}^2$. The term 0.1 represents the squared order parameter associated with the motion around the C$-$CH$_3$ axis, and $S_{\mathrm{axis}}{}^2$ the axial squared order parameter associated with motion of the C$-$CH$_3$ axis. The effective correlation time for local motion, τ_e, has been associated with *both* local motional modes. This yields the spectral density:[10,27b]

$$J^{QQ}(\omega) = S_{\mathrm{axis}}{}^2 0.1\tau_m/(1 + \omega^2\,\tau_m{}^2) + (1 - S_{\mathrm{axis}}{}^2 0.1)\tau_e{}'/(1 + \omega^2\,\tau_e{}'^2) \quad (2)$$

2. The Slowly Relaxing Local Structure (SRLS) Model. The fundamentals of the stochastic coupled rotator slowly relaxing local structure (SRLS) theory[24,25] as applied to biomolecular dynamics[26] have been developed recently for NMR spin relaxation in proteins.[16-23] Two rotators, representing the global motion of the protein, $\boldsymbol{R}^{\mathbf{c}}$, and the local motion of the probe (C$-$D bond in this case), $\boldsymbol{R}^{\mathbf{L}}$, are treated. The motions of the protein and the probe are coupled by a local potential,

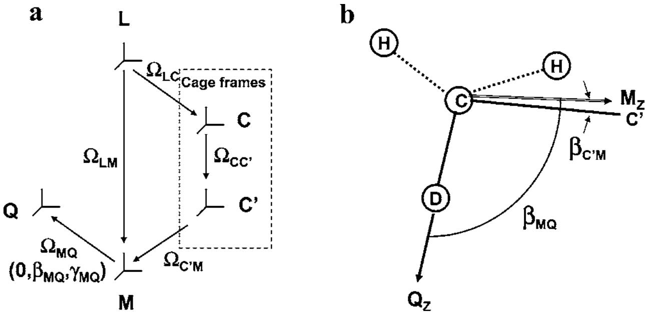

Figure 1. (a) Various reference frames which define the SRLS model: L, laboratory frame; C, global diffusion frame associated with protein shape; C′, local director frame fixed in the protein; M, local ordering/local diffusion frame fixed in the C−D bond; Q, quadrupolar tensor frame along the C−D bond. (b) Application to methyl dynamics. The simple case of motion about the rotation axis of the methyl group is illustrated. The equilibrium orientation of the CH_2D−C bond (C^α−C^β for alanine, C^β−$C^{\gamma 1}$ and C^β−$C^{\gamma 2}$ for valine, etc.) is taken as the local director, C′. The local ordering frame, M, is assumed in this illustration for simplicity to be axially symmetric. M_Z orients preferentially parallel to C′. It also represents the methyl rotation axis, and it is tilted relative to Q_Z, i.e., the C−D bond, at $\beta_{MQ} = 110.5°$ (when $r_{CH} = r_{CD}$ is set equal to 1.115 Å, ref 23). The angle $\beta_{C'M}$ is the stochastic angle between the instantaneous orientation of the M frame, M_Z, and its equilibrium orientation, C′.

$U(\Omega_{C'M})$, where C′ denotes the local director fixed in the protein, and M the local ordering/local diffusion frame fixed in the probe. The Euler angles $\Omega_{C'M}$ are modulated by the local motion whereas the Euler angles $\Omega_{LC'}$, with L denoting the fixed laboratory frame, are modulated by the overall tumbling of the protein.[21] If the protein is considered axially symmetric, then a global diffusion frame C tilted relative to the C′ frame will be defined. The site-specific angles, $\beta_{CC'}$, are fixed in the protein. The various frames entering the SRLS/model and the magnetic quadrupolar frame are shown in Figure 1.

Formally the diffusion equation for the coupled system is given by

$$\frac{\partial}{\partial t}P(X,t) = -\hat{\Gamma}P(X,t) \tag{3}$$

where X is a set of coordinates completely describing the system.

$$X = (\Omega_{C'M},\Omega_{LC'})$$

$$\hat{\Gamma} = \hat{J}(\Omega_{C'M})\boldsymbol{R}^{L}P_{eq}\hat{J}(\Omega_{C'M})P_{eq}{}^{-1} + [\hat{J}(\Omega_{C'M}) - \hat{J}(\Omega_{LC'})]\boldsymbol{R}^{C}P_{eq}[\hat{J}(\Omega_{C'M}) - \hat{J}(\Omega_{LC'})]P_{eq}{}^{-1} \tag{4}$$

where $\hat{J}(\Omega_{C'M})$ and $\hat{J}(\Omega_{LC'})$ are the angular momentum operators for the probe and the protein, respectively.

The Boltzmann distribution $P_{eq} = \exp[-u(\Omega_{C'M})]/\langle\exp[-u(\Omega_{C'M})]\rangle$ is defined with respect to the (scaled) probe−cage interaction potential given by

$$u(\Omega_{C'M}) = \frac{U(\Omega_{C'M})}{k_BT} = -c_0^2D_{0,0}^2(\Omega_{C'M}) - c_2^2[D_{0,2}^2(\Omega_{C'M}) + D_{0,-2}^2(\Omega_{C'M})] \tag{5}$$

This represents the expansion in the full basis set of Wigner rotation matrix elements, $D_{KM}^{L}(\Omega_{C'M})$, with only lowest order, i.e., $L = 2$, terms being preserved.[21,23,25,26] The coefficient c_0^2 (given in units of k_BT) is a measure of the orientational ordering of the C−D bond with respect to the local director, C′, whereas c_2^2 measures the asymmetry of the ordering around the director.

Time correlation functions are calculated as

$$C_{M,KK'}^{J}(t) = \langle D_{M,K}^{J*}(\Omega_{LM})|\exp(-\hat{\Gamma}t)|D_{M,K'}^{J}(\Omega_{LM})P_{eq}\rangle \tag{6}$$

Their Fourier−Laplace transforms yield the spectral densities $j_{M,KK'}^{J}(\omega)$.

In the case of zero potential, $c_0^2 = c_2^2 = 0$, the solution of the diffusion operator associated to the time evolution operator features three distinct eigenvalues for the probe motion:

$$1/\tau_K = 6R_{\perp}^{L} + K^2(R_{\parallel}^{L} - R_{\perp}^{L}) \quad \text{for } K = 0, 1, 2 \tag{7}$$

where $R_{\parallel}^{L} = 1/(6\tau_{\parallel})$ and $R_{\perp}^{L} = 1/(6\tau_{\perp}) = 1/(6\tau_0)$. Only the diagonal terms, $j_K(\omega)$ (the functions $j_{KK'}$ denote the real part of $j_{M,KK'}^{2}$, see ref 25), are nonzero, and they can be calculated analytically as Lorentzian spectral densities, each defined by width $1/\tau_K$. When the ordering potential is axially symmetric, $c_0^2 \neq 0$, $c_2^2 = 0$, again only diagonal terms persist, but they are given by infinite sums of Lorentzian spectral densities which are defined in terms of eigenvalues $1/\tau_i$ of the diffusion operator, and weighing factors $c_{K,i}$, such that

$$j_K(\omega) = \sum_i \frac{c_{K,i}\tau_i}{1 + \omega^2\tau_i^2} \tag{8}$$

The eigenvalues $1/\tau_i$ represent modes of motion of the system, in accordance with the parameter range considered. Note that although in principle the number of terms in eq 8 is infinite, in practice a finite number of terms is sufficient for numerical convergence of the solution.

Finally, when the local ordering potential is rhombic, $c_0^2 \neq 0$, $c_2^2 \neq 0$, both diagonal $j_K(\omega)$ and nondiagonal $j_{KK'}(\omega)$ terms are different from zero and need to be evaluated explicitly according to expressions analogous to eq 8.

The spectral densities $j_{KK'}(\omega)$ are defined in the M frame. If the M frame and the magnetic frame are tilted, a Wigner rotation will be required to obtain the measurable autocorrelated spectral density, $J^{QQ}(\omega)$, from the $j_K(\omega)$ and $j_{KK'}(\omega)$ spectral densities.[40] Because of the additional symmetry $j_{M,K,K'} = j_{M,-K,-K'}$, only the diagonal terms, $j_K(\omega)$, with $K = 0, 1, 2$ and the nondiagonal terms, $j_{KK'}(\omega)$, with $KK' = (-2,2), (-1,1), (-1,2), (0,1), (0,2)$, and $(1,2)$, need to be considered.

For an axial magnetic frame, Q, one has the explicit expression:

$$J^{QQ}(\omega) = d_{00}{}^2(\beta_{MQ})^2j_{00}(\omega) + 2d_{10}{}^2(\beta_{MQ})^2j_{11}(\omega) + 2d_{20}{}^2(\beta_{MQ})^2j_{22}(\omega) + 4d_{00}{}^2(\beta_{MQ})d_{20}{}^2(\beta_{MQ})j_{02}(\omega) + 2d_{-10}{}^2(\beta_{MQ})d_{10}{}^2(\beta_{MQ})j_{-11}(\omega) + 2d_{-20}{}^2(\beta_{MQ})d_{20}{}^2(\beta_{MQ})j_{-22}(\omega) \tag{9}$$

with only the diagonal terms, $j_K(\omega)$, with $K = 0, 1, 2$, and the nondiagonal terms, $j_{KK'}(\omega)$, with $KK' = (0,2), (-1,1)$, and $(-2,2)$ contributing.

A convenient measure of the orientational ordering of the C−D bond is provided by the order parameters, $S_0^2 = \langle D_{00}^2(\Omega_{C'M})\rangle$ and $S_2^2 = \langle D_{02}^2(\Omega_{C'M}) + D_{0-2}^2(\Omega_{C'M})\rangle$, which are related to the orienting potential (eq 5), hence c_0^2 and c_2^2, via the ensemble averages:

$$\langle D_{0n}^2(\Omega_{C'M})\rangle = \frac{\int d\Omega_{C'M}D_{0n}^2(\Omega_{C'M})\exp[-u(\Omega_{C'M})]}{\int d\Omega_{C'M}\exp[-u(\Omega_{C'M})]} \tag{10}$$

One may convert to Cartesian ordering tensor components according to $S_{zz} = S_0^2$, $S_{xx} = (\sqrt{1.5}S_2^2 - S_0^2)/2$, $S_{yy} = -(\sqrt{1.5}S_2^2 + S_0^2)/2$. Note that $S_{xx} + S_{yy} + S_{zz} = 0$.

For ^{2}H relaxation, the measurable quantities are $J^{QQ}(0)$, $J^{QQ}(\omega_D)$, and $J^{QQ}(2\omega_D)$. Together with the squared magnetic quadrupole interaction, they determine the experimentally measured relaxation rates according to standard expressions for NMR spin relaxation.[41,42]

In the present study we allowed for at most four fitting parameters including the potential coefficients c_0^2 and c_2^2, R^c defined in units of R^L (hence representing the time scale separation between the global and local motions) and the "diffusion tilt" β_{MQ}. We used $R^c = {}^1/_6\tau_m$ with τ_m as determined in refs 12 and 43 based on ^{15}N T_1/T_2 ratios.[44] When β_{MQ} is set equal to zero, then the SRLS spectral density is *formally* analogous with the original MF spectral density (eq 1).

The functions $j_K(\omega)$ (eq 8) and $j_{KK'}(\omega)$ (equations analogous to eq 8) are calculated during data fitting on the fly. In the methyl dynamics application, the local potential (the equivalent of S^2 in MF) is low, with $|c_0^2|$ and $|c_2^2|$ on the order of 1−2 (in units of k_BT). The time scale separation, R^c, is also not too large. The computational effort was found to be very reasonable in this case. Thus, it took about 40 min on a 3.2 GHz Pentium 4 processor to fit the relaxation data of a given methyl group of protein L. Our SRLS-based fitting program is similar to the MF fitting programs. The only extra requirement on the part of the user is to determine a truncation parameter, which determines the size of the matrix representation required for convergence of the solution (given by eq 8 or similar equations). Several trial and error calculations carried out for typical parameter sets suffice. Our current software is available upon request. The "theoretical background" sections of this paper and of references 21 and 23 comprise the information required for ab initio programming.

3. MF as SRLS Asymptote. Equation 1, from which eq 2 has been derived, represents the SRLS solution in the Born−Oppenheimer (BO) limit where $\tau_m \gg \tau_e$.[45,46a] Equation 1 was obtained in early work as a perturbational expansion of SRLS in the limit of $\tau_m \gg \tau$ for axial local ordering, isotropic global ($\boldsymbol{R^c}$) and local ($\boldsymbol{R^L}$) diffusion, and collinear magnetic and ordering tensors.[45] In this limit, S^2 represents $(S_0^2)^2$ (eqs 5 and 10 with $c_2^2 = 0$) and τ_e is given by τ_0 of eq 7. When the coupling potential is very high then the phenomenon called renormalization[46b,c] becomes important. The renormalized correlation time, τ_{ren}, is given approximately by $2\tau_0/c_0^2$ where c_0^2 represents the potential coefficient.[46c] We found that in this limit, τ_e agrees with τ_{ren} and S^2 agrees with $(S_0^2)^2$ (references 20 and 21). Outside of the BO limit, eq 1 is not valid for diffusive motion (or wobble-in-a-cone, if the latter is associated with a cosine squared potential) and will consequently lead to force-fitting.

As already noted, eq 2 features two local dynamic modes associated with the axial order parameters, $[P_2(\cos\beta_{MQ})]^2 = [P_2(\cos 110.5°)]^2 = 0.1$ and $S_{axis}{}^2$, for motion *around* and *of* the C−CH$_3$ axis, respectively, and a common correlation time, τ_e. A major inconsistency in eq 2 is having the local ordering/local diffusion axis, M, tilted at 110.5° from the magnetic axis, Q, but ignoring the $K = 1$ and $K = 2$ contributions (eq 8). Independent of the model assumed (e.g., see reference 27a where the Woessner model is being developed), these terms enter the calculation of the exact $J^{QQ}(\omega)$ function as $3\sin^2(110.5°)\cos^2(110.5°)j_1(\omega) = 0.323\, j_1(\omega)$ and $0.75\sin^4(110.5°)j_2(\omega) = 0.577 j_2(\omega)$. Yet, $J^{QQ}(\omega)$ of eq 2 comprises only the $K = 0$ term. This is only valid in the extreme motional narrowing limit[23] where $R_\perp^L = R^c$ and $R_\parallel^L \to \infty$ (eq 7, ref 26; see also eq 31 of ref 27c and pertinent discussion). The condition that $R_\parallel^L \to \infty$ (equivalent to $\tau_e \to 0$ in MF) renders the functions $j_1(\omega)$ and $j_2(\omega)$ so small that the $K = 1$ and $K = 2$ terms can be ignored. When $\tau_e \to 0$, the second term of eq 2 can be ignored to obtain $J^{QQ}(\omega) = (1.5\cos^2(110.5°) - 0.5)^2 j_0(\omega) = 0.1 j_0(\omega)$, where $j_0(\omega) = S_{axis}{}^2\tau_m/(1 + \omega^2\tau_m{}^2)$. It can be seen that in this limit the effect of the local motional modes consists of reducing the quadrupole interaction (featured by the relaxation rate expressions) consecutively by 0.1 and $S_{axis}{}^2$.

In practice combined ^{2}H T_1 and T_2 autocorrelated relaxation rates *cannot be fit* from a statistical point of view with τ_e set equal to zero in eq 2 because the extreme motional narrowing limit has not been attained. Technically the data *can often be fit* with $\tau_e \neq 0$. However, in this case the quantities $S_{axis}{}^2$ and τ_e have only vague physical meaning and, as shown below, they provide a distorted picture of the actual situation if taken seriously.

III. Results and Discussion

In principle one should first consider axial local potentials in the SRLS fitting process. We showed previously[23] that this leads to a physically problematic picture and implies inconsistencies between ^{2}H autocorrelation in ^{13}CDH$_2$ (ref 12) and HC−HH cross-correlation in ^{13}CH$_3$ (ref 43). The problems mentioned have been resolved by allowing for rhombic potentials.[23] Therefore in this study we allow for rhombic potentials from the start.

The Form of $J^{QQ}(\omega)$ for Methyl Dynamics. The SRLS model yields the generic spectral densities, $j_{KK'}(\omega)$. The measurable spectral density, $J^{QQ}(\omega)$, is given by linear combinations of the relevant $j_{KK'}(\omega)$ functions. The symmetry of the local ordering (M frame) determines which KK' quantum numbers are nonzero, and, together with the other physical parameters, the $j_{KK'}(\omega)$ functions. The orientation of the M frame with respect to the magnetic quadrupolar frame determines the coefficients in the linear combination yielding $J^{QQ}(\omega)$ (eq 9). For a rhombic M frame and $\beta_{MQ} = 110.5°$, $J^{QQ}(\omega)$ features large contributions from $j_{00}(\omega)$, $j_{22}(\omega)$, and $j_{20}(\omega)$ and smaller contributions from $j_{11}(\omega)$, $j_{2-2}(\omega)$, and $j_{1-1}(\omega)$ (eq 9). $J^{QQ}(0)$, $J^{QQ}(\omega_D)$, and $J^{QQ}(2\omega_D)$ enter the expressions for the ^{2}H spin relaxation rates.

The appropriate representation of methyl dynamics by $J^{QQ}(\omega)$ makes possible the determination of physical parameters (in general, $\boldsymbol{R^L}$, $\boldsymbol{R^c}$, β_{MQ}, c_0^2, and c_2^2) despite the fact that relatively few values of $J^{QQ}(\omega)$ are available at any given magnetic field. As pointed out above, unlike heteronuclear ^{15}N−^{1}H and ^{13}C−^{1}H spin relaxation, ^{2}H spin relaxation does not feature high-frequency values of $J(\omega)$, with ω on the order of ω_H. Choy and Kay[47] have shown that even with twenty *synthetic* data points (^{2}H T_1, T_2 and three relaxation rates associated with rank 2 coherences generated at 9.4, 11.7, 14.1, and 18.8 T) the results of fitting these data with a model-free spectral density were unacceptable. Only further parametrization of this function yielded statistically acceptable results by force fitting.

We illustrate below typical SRLS spectral densities used in methyl dynamics analysis (Figures 2−4). Figure 2 shows the $j_{KK'}(\omega)$ functions calculated using a typical parameter set (obtained by analyzing the data acquired for methyl T23 of protein L at magnetic fields of 9.4, 11.7, 14.1, and 18.8 T, 25 °C) featuring $c_0^2 = 1.82$, $c_2^2 = -0.67$ and $R^c = 0.017$. Note that R^c is given in units of R^L. Hence 0.017 represents the ratio between the global and local motional rates. Since the global

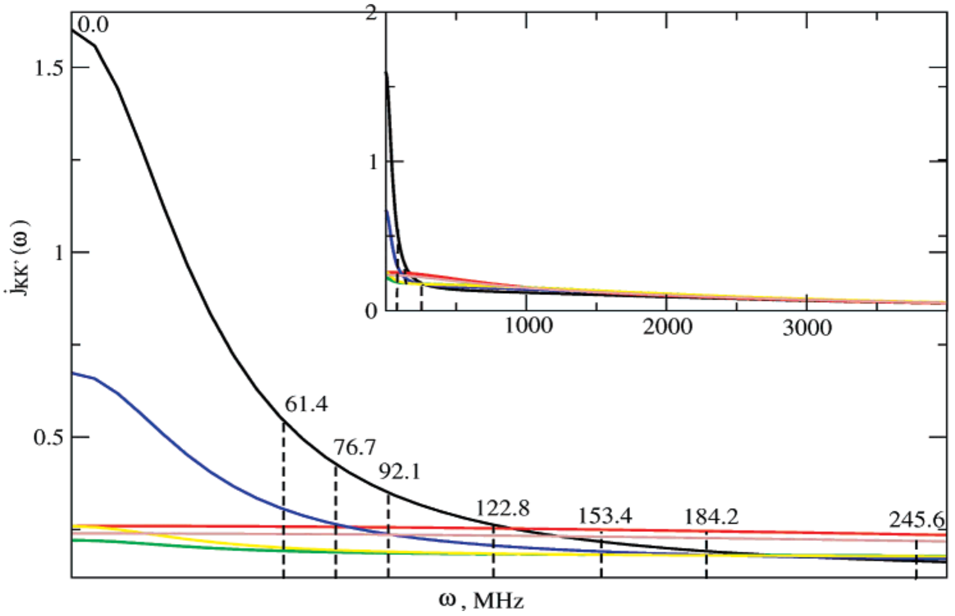

Figure 2. $j_{KK'}(\omega)$ functions with $KK' = (0,0)$, black; (1,1), red; (2,2), green; (2,0), blue; (2,−2), yellow; and (1,−1), brown calculated with eq 8 and an analogous equation appropriate for cross-terms, using $c_0^2 = 1.82$, $c_2^2 = -0.67$, and $R^c = 0.017$, which are the best-fit SRLS parameters obtained for methyl T23 at 25 °C. The inset shows a compressed ω-range extending from 0 to 4000 MHz. $j_{KK'}(\omega)$ is given in units of $1/R^L$ and ω is given in units of R^L.

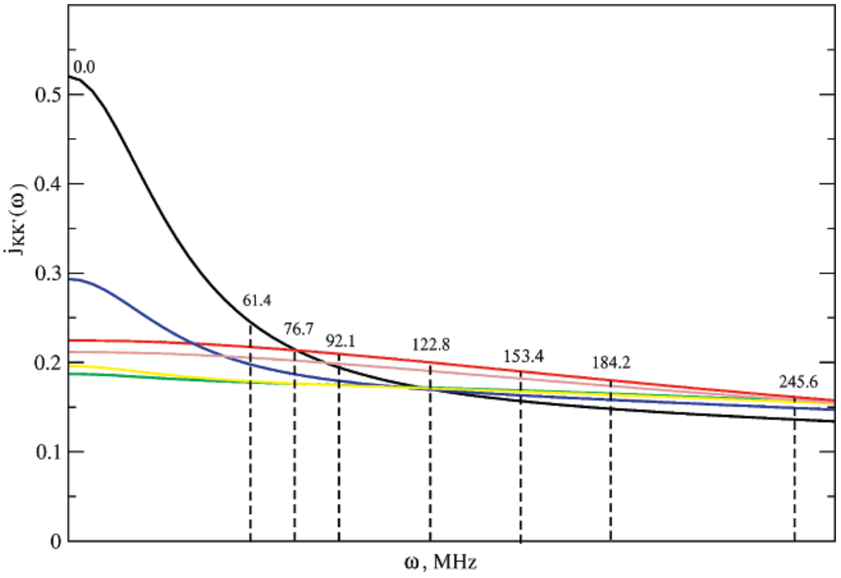

Figure 3. $j_{KK'}(\omega)$ functions with $KK' = (0,0)$, black; (1,1), red; (2,2), green; (2,0), blue; (2,−2), yellow; and (1,−1), brown calculated with eq 8 and an analogous equation appropriate for cross-terms, using $c_0^2 = 1.5$, $c_2^2 = -0.5$, and $R^c = 0.05$. $j_{KK'}(\omega)$ is given in units of $1/R^L$ and ω is given in units of R^L.

motional rate is known independently, the parameter R^c actually determines the local motional rate. The inset shows a compressed ω-range extending from 0 to 4000 MHz, and the extreme ω-values of 61.4 and 245.6 MHz. Clearly the portion of the $j_{KK'}(\omega)$ functions sampled consist of a restricted region outside of which these functions are not defined experimentally. Note that the magnetic field range scanned in Figure 2 is almost as large as feasible with currently available technology. Figure 3 shows the $j_{KK'}(\omega)$ functions calculated for $c_0^2 = 1.5$, $c_2^2 = -0.5$, and $R^c = 0.05$, and Figure 4 shows the $j_{KK'}(\omega)$ functions of Figure 3 assembled into $J^{QQ}(\omega)$ for $\beta_{MQ} = 69.5°$ (the complement of 110.5°; the time correlation functions (eq 6) are the same for β_{MQ} and $(180° - \beta_{MQ})$). While SRLS fitting needs to account for the various $j_{KK'}(\omega)$ functions (e.g., Figures 2 and 3) and their coefficients, model-free only needs to reproduce specific values of the $J^{QQ}(\omega)$ function (e.g., Figure 4) because the MF spectral density is a parametrized version of the actual measurable spectral density. We found that SRLS and MF spectral densities, which are formally equivalent, yield best-fit parameters with significantly smaller uncertainties in the SRLS scenario.

Fitting Strategy and Error Estimation. Exhaustive grid searches are impractical with SRLS. To ascertain that the global minimum of the least-squares sum (LSS) “target” function has been reached in a given fitting process, we tested various strategies. It was found effective to carry out a coarse grid search, where c_0^2, c_2^2, R^c, and β_{MQ} were allowed to vary, with the starting value of β_{MQ} in the vicinity of the tetrahedral angle, followed by a finer grid search. This strategy was superior to one where β_{MQ} was fixed at the tetrahedral angle value. In general the minimization converged for numerical reasons to $(180° - \beta_{MQ})$ (which, as indicated above, yields the same time correlation functions as β_{MQ}). To facilitate comparison of

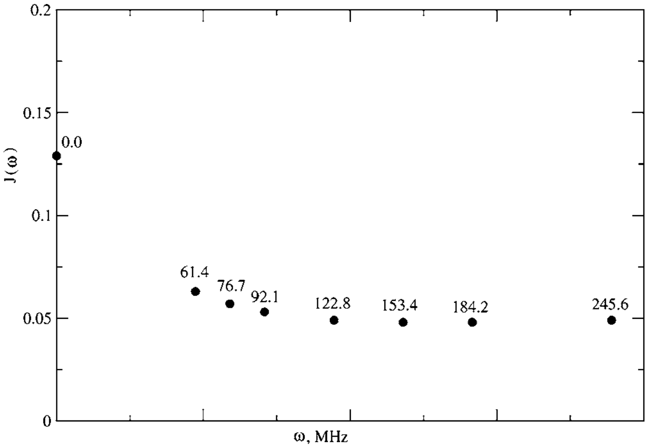

Figure 4. $J^{QQ}(\omega)$ function assembled from the $j_{KK'}(\omega)$ functions shown in Figure 3, using $\beta_{MQ} = 69.5°$. $J(\omega)$ is given in units of $1/R^L$ and ω is given in units of R^L.

TABLE 1: Best-Fit Parameters, Listed under "Output", Obtained with Combined Fitting of 16 Relaxation Rates (8 Relaxation Rates Including ^{2}H T_1 and T_2 Acquired at 9.4, 11.7, 14.1, and 18.8 T and 6 Relaxation Rates Associated with the Three Rank 2 Coherences Acquired at 11.7 and 14.1 T) Measured at 25 °C for Methyl A50, Using the Input Parameters Shown under "Input" (Rows 1−6), Using Only ^{2}H T_1 and T_2 Data (Rows 7−12), the τ_m Value Used Was 4.05 ns,[12] χ^2_{red} Values Are Also Shown, the Local Motional Rate Is Given by $R^c \times \tau_m$

	input		output		
	c_0^2	R^c	c_0^2	R^c	χ^2_{red}
1	0.5	0.0035	0.88	0.0038	7
2	0.89	0.0035	0.88	0.0037	7
3	1.2	0.0035	0.88	0.0038	7
4	0.5	0.008	0.88	0.0038	7
5	0.89	0.008	0.89	0.0037	7
6	1.2	0.008	0.88	0.0038	7
7	0.5	0.0035	0.84	0.0038	0.1
8	0.89	0.0035	0.84	0.0039	0.2
9	1.2	0.0035	0.84	0.0038	0.1
10	0.5	0.008	0.85	0.0038	0.1
11	0.89	0.008	0.85	0.0038	0.1
12	1.2	0.008	0.85	0.0038	0.1

potential coefficients among methyl groups, we fixed β_{MQ} at 69.5° in the final calculation for each methyl group. An alternative (more tedious) strategy, which yielded very similar but not identical results, consisted of allowing β_{MQ} to vary freely and accepting only those sets of temperature-dependent fits where β_{MQ} was within half a degree of 69.5°. Clearly it is necessary to devise an effective automated fitting protocol based on *both statistical and physical criteria.* This effort is underway.

Both procedures outlined above comprise error estimation capabilities, which can be used in different ways. The Monte Carlo-based error estimation methods used in MF-based fitting,[48] which would involve hundreds of calculations of $J^{QQ}(\omega)$, are not practical with SRLS. In ref 12 a strategy where part of the experimental data was eliminated systematically was used to evaluate uncertainties. Ultimately we used a combination of the various methods mentioned to estimate the errors in the best-fit parameters, found to be typically on the order of 10%.

TABLE 2: Combined Fitting of 10 Relaxation Rates (^{2}H T_1, T_2, and the Three Relaxation Rates Associated with the Rank 2 Coherences) Acquired at 11.7 and 14.1 T, 25 °C for the Depicted Methyl Groups, the Data Under "MF" Were Taken From Ref 12, The Penultimate and Ultimate Columns on the Right Show $R(c_0^2) = c_0^2(\mathrm{SRLS})/c_0^2(\mathrm{MF})$ and $R(\tau) = \tau_0(\mathrm{SRLS})/\tau_e(\mathrm{MF})$, Respectively, the Residues Marked in Boldface Required an Extended MF Formula for Data Analysis.[12]

	MF				SRLS					
methyl	$S_{axis}{}^2$	c_0^2	τ_e, ps	R^c	c_0^2	c_2^2	τ_0, ps	R^c	$R(c_0^2)$	$R(\tau)$
V2γ_1	0.73	1.22	54	0.013	1.77	−0.82	101	0.025	1.5	1.9
T37	0.74	1.23	50	0.012	1.89	−0.92	97	0.024	1.5	1.9
T55	0.98	1.41	51	0.012	1.83	−0.95	113	0.028	1.3	2.2
T17	0.97	1.42	45	0.011	1.56	−0.82	117	0.029		
I9δ	0.38	0.89	24	0.006	1.57	−0.50	28	0.007	1.8	1.2
L8δ_1	0.30	0.79	35	0.009	−0.29	−0.50	53	0.013		
L8δ_2	0.30	0.79	41	0.010	−0.35	−0.50	57	0.014		
T15	0.57	1.09	69	0.017	1.79	−0.95	105	0.026	1.6	1.5
L38δ_1	0.56	1.08	34	0.008	1.68	−0.74	61	0.015	1.6	1.8
V47γ_1	0.57	1.09	55	0.014	1.51	−0.58	93	0.023	1.4	1.7
I58δ	0.58	1.10	17	0.004	1.86	−0.56	32	0.008	1.7	1.9
V49γ_2	0.62	1.13	40	0.010	1.68	−0.82	61	0.015	1.5	1.5
L56δ_1	0.61	1.12	70	0.017	1.89	−1.09	117	0.029	1.7	1.7
L56δ_2	0.61	1.12	38	0.009	1.60	−0.68	65	0.016	1.4	1.7
A61	0.60	1.11	46	0.011	1.68	−0.73	77	0.019	1.5	1.7
T3	0.88	1.33	39	0.010	1.78	−0.89	85	0.021	1.3	2.2
T28	0.88	1.33	41	0.010	1.82	−1.02	85	0.021	1.4	2.1
I4γ	0.87	1.32	24	0.006	1.84	−0.78	73	0.018	1.4	3.1
A33/A11	0.89	1.34	37	0.009	1.87	−0.91	101	0.025	1.4	2.7
A11/A33	0.82	1.29	49	0.012	1.98	−1.02	134	0.033	1.5	2.7
A18	0.81	1.28	57	0.014	1.90	−1.00	109	0.027	1.5	1.9
I58γ	0.82	1.29	27	0.007	1.79	−0.96	53	0.013	1.4	2.0
T46	0.69	1.20	63	0.016	1.89	−1.00	105	0.026	1.6	1.7
V49γ_1	0.68	1.18	34	0.008	1.72	−0.68	69	0.017	1.5	2.0
T23	0.84	1.31	39	0.010	1.84	−0.94	81	0.020	1.4	2.1
A50	0.84	1.31	24	0.006	1.81	−0.93	53	0.013	1.4	2.2
A31	0.83	1.30	77	0.019	1.94	−1.15	134	0.033	1.5	1.7

Importance of the Rank 2 Coherences. Including the rank 2 coherences into the experimental data set increases the accuracy of the results, obviously with a higher but still acceptable reduced χ^2 value. This is illustrated in Table 1, using for simplicity axial potentials. It can be seen that practically the same results are obtained independent of the starting values with 16 data points, 8 of which are relaxation rates associated with the rank 2 coherences (rows 1−6). Using 8 data points comprising only the ^{2}H T_1 and T_2 relaxation rates yields $(S_0^2)^2$ values lower by 4.8% (rows 7−12). The discrepancies are parameter-range dependent (not shown).

A difference of 4.8% in $S_{axis}{}^2$ implies differences in the potential coefficient, c_0^2, exceeding 20%, due to the shape of the squared order parameter *versus* c_0^2 function for high $(S_0^2)^2$ values. This has been discussed in detail in ref 21. Note that Table 1 features an illustrative example. In general the differences between corresponding best-fit parameters determined with rank 2 coherences included or excluded might be larger.

Qualitative MF-Based Information. We checked whether adequate *qualitative* information could be obtained with MF. The parameter used in MF to estimate the strength of the local spatial restrictions is $S_{axis}{}^2$. The SRLS parameter, which serves the same purpose, is the coefficient, c_0^2, obtained with axial-potential-based data fitting. Table 2 shows groups of methyl moieties with very similar $S_{axis}{}^2$ values and the corresponding best-fit SRLS parameters. Ten data points (^{2}H T_1, T_2 and the three relaxation rates associated with the rank 2 coherences acquired at 11.7 and 14.1 T and 25 °C) have been used as experimental data set. The MF data shown in Table 2 were taken from ref 12. We also show c_0^2(MF) derived from $S^2 = 0.1 \times S_{axis}{}^2$ using the axial versions of eqs 5 and 10. The penultimate and ultimate columns on the right show $R(c_0^2) = c_0^2(\mathrm{SRLS})/c_0^2(\mathrm{MF})$ and $R(\tau) = \tau_0(\mathrm{SRLS})/\tau_e(\mathrm{MF})$, respectively. It can be seen that these ratios are larger than unity and in many cases

TABLE 3: Best-Fit Parameters Obtained with Combined Fitting of 5 Relaxation Rates (^{2}H T_1, T_2, and the Three Relaxation Rates Associated with the Rank 2 Coherences) Acquired at 11.7 T, 5 °C, for the Depicted Methyl Groups, the Global Motion Correlation Time Used Was $\tau_m = 8.01$ ns,[12,43] the Quadrupole Interaction Was 167 kHz, and the $r_{CH} = r_{CD}$ Distance 1.115 Å, All the c_2^2/c_0^2 Values Are Negative

methyl	c_0^2	c_2^2	R^c	τ_0, ps	$\lvert c_2^2/c_0^2\rvert$
L8δ_1	1.49	−0.20	0.014	112	0.13
L38δ_1	1.51	−0.33	0.012	96	0.22
L56δ_2	1.54	−0.22	0.015	120	0.14
T55	1.19	−2.66	0.004	32	2.24
T23	1.53	−0.28	0.016	128	0.18
A18	1.37	−1.66	0.013	104	1.21
A50	1.51	−0.77	0.010	80	0.51
L38δ_2	1.50	−0.51	0.014	112	0.34
T37	1.51	−0.65	0.027	216	0.43
T17	1.92	−1.69	0.019	152	0.88
V49γ_2	1.62	−0.85	0.012	96	0.59
A6	1.55	−0.92	0.020	160	0.59
A61	1.51	−0.95	0.013	104	0.63
V47γ_1	1.51	−0.61	0.016	128	0.40
V2γ_2	1.56	−0.82	0.012	100	0.53
I9γ	1.56	−0.80	0.012	96	0.50

vary considerably within a given group of similar S_{axis}^2 values, indicating that the variations in S_{axis}^2(MF) and c_0^2(SRLS) are likely to differ qualitatively.

Profiles of c_0^2(SRLS) (based on the best-fit parameters obtained with SRLS at 5 and 25 °C for the methyl groups of Tables 3 and 5) and the corresponding S_{axis}^2(MF) values (taken from ref 12) are shown in Figure 5. For clarity, the methyl groups have been classified as follows. SRLS categories 1, 2, and 3 correspond to $c_0^2 > 1.65$, $1.49 \le c_0^2 \le 1.65$, and $c_0^2 < 1.49$, ($c_0^2 > 1.80$, $1.60 \le c_0^2 \le 1.80$, and $c_0^2 < 1.60$) at 5 (25) °C. MF categories 1, 2, and 3 correspond to $S_{axis}^2 > 0.85$, $0.6 \le S_{axis}^2 \le 0.85$, and $S_{axis}^2 < 0.6$ ($S_{axis}^2 > 0.89$, $0.6 \le S_{axis}^2 \le 0.89$, and $S_{axis}^2 < 0.6$) at 5 (25) °C. Clearly the c_0^2 and S_{axis}^2 profiles differ significantly, often exhibiting opposite trends at the same temperature, and different temperature dependences.

Hence, care is to be exerted in MF analyses in interpreting squared order parameters and local motion correlation times in terms of physical or biological properties. S_{axis}^2 has been used extensively to derive residual configurational entropy and heat capacity, with far-fetched implications.[30] Recently a new term called, "polar dynamics", based on relative S_{axis}^2 values, was set forth.[49] Small differences in S_{axis}^2 and τ_e (which is actually a composite depending on both S^2 and a bare rate of local motion) have been used to elucidate communication pathways in proteins.[50] Such inferences require accurate best-fit parameters.

Data Fitting. Five relaxation rates (^{2}H T_1 and T_2, and relaxation rates associated with two-quantum, two-spin order and antiphase rank 2 coherences) acquired at 5, 15, 25, 35, and 45 °C, 11.7 T, have been measured for the methyl groups L8δ_1, L38δ_1, L56δ_2, T55, T23, A18, A50, L38δ_2, T37, T17, V49γ_2, A6, A61, V47γ_1, V2γ_2, and I9γ. These data were fit with SRLS allowing c_0^2, c_2^2, and R^c to vary while (ultimately) keeping β_{MQ} fixed at 69.5°. The best-fit parameters are shown in Tables 3−7.

The results of fitting the data acquired at 5 °C, shown in Table 3, feature best-fit R^c values of 0.01−0.02 (with the exception of methyl T55). The coefficient of the axial term of the local potential, c_0^2, is approximately 1.5 in units of k_BT. The potential asymmetry (rhombicity), as given by $\lvert c_2^2/c_0^2\rvert$ lies within the range of 0.13−0.63 (with the exception of methyl groups T55, A18, and T17). Inspection of the data shown in Tables 4−7, obtained at the higher temperatures, points to a diversified picture. We present in Table 8 results obtained by averaging over the methyl groups analyzed at any given temperature. It can be seen that *on average* R^c increases, τ_0 decreases, c_0^2 increases, c_2^2 decreases, and $\lvert c_2^2/c_0^2\rvert$ decreases with increasing temperature.

Decrease in the local motional correlation time, τ_0, with increasing temperature is expected. An activation energy of 2 ± 0.2 kcal/mol has been derived from the data of Table 8 based on the Arrhenius relation for the rate $1/(6\tau_0)$. Large site-specific variations in local motional correlation times of methyl groups in proteins have been predicted theoretically.[27b,51] The value of 2 kcal/mol pertains to the theoretically predicted range, and the 10-fold lower SRLS rates are in significantly better agreement with the theoretical predictions than the MF rates.[27b,51]

On the basis of the Arrhenius relation for the rate $1/(6\tau_m)$ (with τ_m determined previously[12,43]) we obtained an activation energy of 6.72 ± 0.36 kcal/mol for the global motion of protein L, in agreement with similar values obtained for other proteins in aqueous solution (see ref 22 and relevant papers cited therein).

Mode-coupling, as expressed by the parameter $\langle R^C\rangle = \langle \tau_0/\tau_m\rangle$, increases with increasing temperature, in accordance with the activation energies for global and local motion. This is an interesting result further documented below by outlining the mode-composition at various temperatures.

The asymmetry of the local potential, as expressed by $\langle\lvert c_2^2/c_0^2\rvert\rangle$, decreases with increasing temperature. This is also interesting new information indicating that the local spatial restrictions at the site of the motion of the methyl group become more axially symmetric as the temperature is raised.

When the local potential is axially symmetric and $\beta_{MQ} = 110.5°$ (with $r_{CH} = r_{CD} = 1.115$ Å) the local spatial restrictions at the methyl site are characterized by c_0^2, which evaluates the potential strength. Clearly c_0^2 is expected to decrease with increasing temperature. When the potential is rhombic and β_{MQ} is also allowed to vary, the *set* of parameters c_0^2, c_2^2, and β_{MQ}, rather than c_0^2 alone, evaluates the local restrictions. Changes in c_0^2 with temperature represent in this case *apparent* changes in potential strength.

Intersite comparison of the local restrictions based on parameter sets is not straightforward. We have been looking for simplified models, which evaluate this important aspect of methyl dynamics in a more direct manner. The combination where c_0^2 is fixed at its Woessner-model-compatible value and β_{MQ} at 110.5°, with c_2^2 and the local motion correlation time, τ, allowed to vary, was found to be appropriate. It yields results, which are similar at lower temperatures and very close at higher temperatures, to those of the complete model. The parameter τ decreases consistently with increasing temperature, as required by physical viability, and $\lvert c_2^2\rvert$ decreases with increasing temperature in most cases. The typical decrease (exceptional increase) in structural rhombicity at most (specific) methyl sites with increasing temperature constitutes interesting new information. These developments will be reported shortly elsewhere.

Temperature-Dependent Mode Composition. We illustrate the mode-coupling concept inherent to the SRLS model. The "pure", i.e., unrestricted by a potential local motional mode has an eigenvalue of 6, and the "pure" global motional mode has an eigenvalue of $6R^C$, both in units of R^L.[24] In the original MF formula (eq 1), which is a limiting case of the two coupled rotator model,[20,21,24,45] the weighting factors of the global and

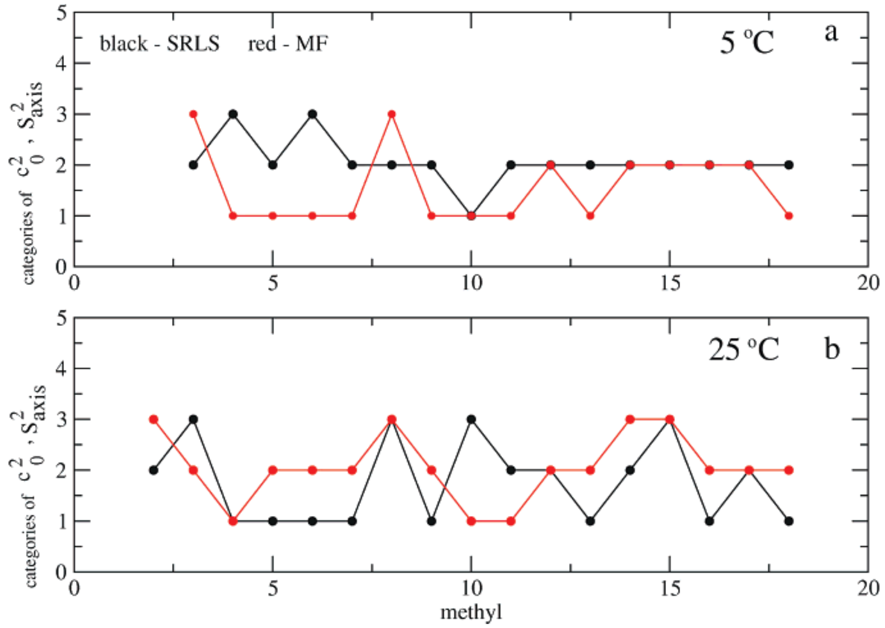

Figure 5. Schematic representing trends in c_0^2 SRLS and $S_{\text{axis}}{}^2$ MF at 5 °C (a) and 25 °C (b). The c_0^2 and $S_{\text{axis}}{}^2$ values have been classified into three groups according to their magnitude, as outlined in the text. These categories are denoted as 1, 2, and 3 on the ordinate. As pointed out above, the average error in c_0^2 has been estimated at 10%. A conservative estimate of the average error in $S_{\text{axis}}{}^2$, based on ref 12, is 4%. These figures translate into an average error margin of ± 1.5 times the black symbol size and on the order of the red symbol size for the SRLS and MF representations, respectively.

TABLE 4: Best-Fit Parameters Obtained with Combined Fitting of 5 Relaxation Rates (^{2}H T_1, T_2, and the Three Relaxation Rates Associated with the Rank 2 Coherences) Acquired at 11.7 T, 15 °C, for the Depicted Methyl Groups, the Global Motion Correlation Time Used Was τ_m = 5.36 ns,[12,43] the c_2^2/c_0^2 Values Are Negative, Except for Those Marked with Asterisks

methyl	c_0^2	c_2^2	R^c	τ_0, ps	$\lvert c_2^2/c_0^2\rvert$
L8δ_1	1.63	−0.67	0.012	64	0.41
L38δ_1	−0.11	−0.51	0.011	59	4.64*
L56δ_2	1.58	−0.80	0.015	80	0.51
T55	1.66	−0.77	0.024	129	0.46
T23	1.65	−0.77	0.024	129	0.47
A18	1.68	−0.82	0.018	97	0.49
A50	1.64	−0.80	0.013	70	0.49
L38δ2	1.44	+0.35	0.016	86	0.24*
T37	1.77	−0.88	0.022	118	0.50
T17	1.66	−0.80	0.019	102	0.48
T3	1.58	−0.78	0.025	200	0.49
V49γ_2	1.61	−0.71	0.018	97	0.44
A6	1.64	−0.81	0.019	102	0.49
A61	1.64	−0.81	0.013	70	0.49
V47γ_1	1.54	−0.68	0.016	85	0.44
V2γ_2	0.99	−0.99	0.024	129	1.00
I9γ	1.54	−0.61	0.015	80	0.40

TABLE 5: Best-Fit Parameters Obtained with Combined Fitting of 5 Relaxation Rates (^{2}H T_1, T_2, and the Three Relaxation Rates Associated with the Rank 2 Coherences) Acquired at 11.7 T, 25 °C, for the Depicted Methyl Groups, the Global Motion Correlation Time Used Was τ_m = 4.05 ns,[12,43] the c_2^2/c_0^2 Values Are Negative Except for c_2^2/c_0^2 of L8δ_1, Marked with an Asterisk

methyl	c_0^2	c_2^2	R^c	τ_0, ps	$\lvert c_2^2/c_0^2\rvert$
L8δ_1	−0.29	−0.50	0.013	53	1.72*
L38δ_1	1.68	−0.74	0.015	61	0.44
L56δ_2	1.60	−0.68	0.016	65	0.43
T55	1.83	−0.95	0.028	113	0.52
T23	1.84	−0.94	0.020	81	0.51
A18	1.90	−1.0	0.027	109	0.53
A50	1.81	−0.93	0.013	53	0.51
L38δ_2	1.44	−0.46	0.017	70	0.32
T37	1.89	−0.92	0.024	97	0.49
T17	1.56	−0.82	0.029	118	0.53
T3	1.78	−0.89	0.021	113	0.50
V49γ_2	1.68	−0.82	0.015	61	0.52
A6	1.98	−1.02	0.033	134	0.52
A61	1.68	−0.73	0.019	77	0.43
V47γ_1	1.51	−0.58	0.023	93	0.38
V2γ_2	1.80	−0.79	0.018	73	0.44
I9γ	1.69	−0.78	0.015	61	0.46
A31	1.94	−1.15	0.033	134	0.59

local motional modes correspond to $(S_0^2)^2$ and $(1 - (S_0^2)^2)$, respectively.

When the mode-decoupling limit is exceeded, quite a few modes contribute to the spectral density (eq 8). We show in Table 9 the dynamic modes associated with methyl I9γ at 5, 25, and 45 °C with fractional contributions to the time correlation functions $C_0(t)$, $C_1(t)$, and $C_2(t)$ exceeding 0.1 (the labels 0, 1, and 2 are abridged versions of $KK' = (0,0)$, $(1,1) = (-1,-1)$ and $(2,2) = (-2,-2)$, eq 6). We focus first on $C_0(t)$. For the largest time scale separations of $R^c = 0.012$, and a rhombic potential with $c_0^2 = 1.56$ and $c_2^2 = -0.80$ obtained for I9γ at 5 °C, three major local motional modes with eigenvalues in the vicinity of 6 make a fractional contribution of 0.755. The eigenvalue of the global motion mode (shown in boldface numbers) is equal to the “pure” eigenvalue of $0.072 = 6 \times 0.012$ and the fractional contribution of this mode is 0.092. Additional modes with eigenvalues ranging from 4.87 to 9.17, with various individual weights, contribute 0.064. The rest(0.089) is contributed by a large number of mixed modes with individual weighting factors below 0.1 (not shown). It can be seen that the two-mode limit is exceeded even though the time scale separation is relatively high ($R^c = 0.012$) and the potential relatively weak (c_0^2= 1.56 in units of k_BT).

For $R^c = 0.015$, c_0^2= 1.69, and $c_2^2 = -0.78$, obtained for I9γ at 25 °C, three local motional modes with eigenvalues relatively close to 6 make a combined fractional contribution of 0.767. The global motion eigenvalue is given by $0.090 = 6 \times 0.016$, which is again equal to the “pure” eigenvalue. Its contribution

TABLE 6: Best-Fit Parameters Obtained with Combined Fitting of 5 Relaxation Rates (^{2}H T_1, T_2, and the Three Relaxation Rates Associated with the Rank 2 Coherences) Acquired at 11.7 T, 35 °C, for the Depicted Methyl Groups, the Global Motion Correlation Time Used Was $\tau_m = 2.55$ ns,[12,43] the c_2^2/c_0^2 Values Are Negative Except for c_2^2/c_0^2 of L38δ_1, Marked with an Asterisk

methyl	c_0^2	c_2^2	R^c	τ_0, ps	$\lvert c_2^2/c_0^2\rvert$
L8δ_1	1.49	−0.50	0.017	43	0.36
L38δ_1	−0.54	−0.56	0.015	38	1.04*
L56δ_2	1.46	−0.50	0.020	51	0.34
T55	1.99	−0.66	0.037	94	0.33
T23	2.17	−0.63	0.029	71	0.29
A18	2.09	−0.74	0.039	100	0.35
A50	2.41	−0.55	0.026	66	0.23
L38δ_2	1.19	−0.52	0.016	41	0.44
T37	1.89	−0.58	0.032	82	0.31
T17	1.61	−0.54	0.040	102	0.30
T3	2.12	−0.62	0.030	122	0.29
V49γ_2	1.83	−0.51	0.021	54	0.28
A6	2.06	−0.80	0.042	107	0.39
A61	1.67	−0.51	0.024	61	0.31
V47γ_1	1.59	−0.51	0.029	74	0.32
V2γ_2	1.75	−0.94	0.058	147	0.54
I9g	1.88	−0.90	0.044	112	0.41
A31	1.91	−0.92	0.044	112	0.48

TABLE 7: Best-Fit Parameters Obtained with Combined Fitting of 5 Relaxation Rates (^{2}H T_1, T_2, and the Three Relaxation Rates Associated with the Rank 2 Coherences) Acquired at 11.7 T, 45 °C, for the Depicted Methyl Groups, the Global Motion Correlation Time Used Was $\tau_m = 1.74$ ns,[12,43] the c_2^2/c_0^2 Values Are Negative

methyl	c_0^2	c_2^2	R^c	τ_0, ps	$\lvert c_2^2/c_0^2\rvert$
L8δ_1	0.87	−0.32	0.018	31	0.37
L38δ_1	1.39	−0.50	0.020	35	0.36
L56δ_2	1.93	−0.58	0.007	12	0.30
T55	3.94	−1.18	0.063	110	0.30
T23	4.10	−0.66	0.067	117	0.16
A18	2.68	−0.70	0.052	91	0.26
A50	3.05	−0.54	0.034	59	0.18
L38δ_2	1.49	−0.50	0.015	26	0.34
T37	2.51	−0.57	0.044	77	0.23
T17	2.15	−0.48	0.022	38	0.22
T3	3.06	−0.59	0.049	125	0.19
V49γ_2	2.03	−0.49	0.024	42	0.24
A6	2.48	−0.74	0.058	101	0.30
A61	2.36	−0.44	0.028	49	0.19
V47γ_1	1.96	−0.49	0.034	59	0.25
V2γ_2	2.20	−0.47	0.030	52	0.21
I9γ	2.42	−0.74	0.061	106	0.31
A31	2.03	−1.00	0.050	87	0.49

TABLE 8: Average Best-Fit c_0^2 Values, Rhombicity Ratios $|c_2^2/c_0^2|$, Local Motion Correlation Times, τ_0, and Time Scale Separations, R^c, Obtained for the Methyl Groups in Tables 3−7, the Global Motion Correlation Times, τ_m, Are Also Given

t, °C	$\langle c_0^2\rangle$	$\langle\lvert c_2^2/c_0^2\rvert\rangle$	$\langle\tau_0\rangle$, ps	$\langle R^c\rangle$	τ_m, ns[12,43]
5	1.52	0.60	114	0.014	8.01
15	1.68	0.46	101	0.019	5.36
25	1.74	0.48	88	0.022	4.05
35	1.83	0.36	84	0.033	2.55
45	2.37	0.27	71	0.041	1.74

TABLE 9: Eigenvalues, $1/\tau_i$ (in Units of R^L), and Weighting Factors, $c_{K,i}$, of the SRLS Solution for $C_0(t)$, $C_1(t)$, and $C_2(t)$ Obtained Using (a) $c_0^2 = 1.56$, $c_2^2 = -0.80$, and $R^c = 0.012$, (b) $c_0^2 = 1.69$, $c_2^2 = -0.78$, and $R^c = 0.015$, and (c) $c_0^2 = 2.42$, $c_2^2 = -0.74$, and $R^c = 0.061$, These Values Represent the Best-Fit Parameters Obtained with Rhombic Potential Fitting Using the Data Acquired at a Magnetic Field of 11.7 T and at 5, 25, and 45 °C, Respectively, for Methyl I9γ, In All Cases Shown $\beta_{MQ} = 69.5°$, the Global Motion Mode Is Marked in Boldface

a		b		c	
$1/\tau_i$	$c_{K,i}$	$1/\tau_i$	$c_{K,i}$	$1/\tau_i$	$c_{K,i}$
		$C_0(t)$			
5.30	0.297	5.40	0.309	6.29	0.396
5.94	0.264	6.06	0.270	9.46	0.130
7.92	0.194	8.08	0.188	7.41	0.123
8.08	0.057	8.23	0.050	19.83	0.023
4.87	0.031	4.83	0.024	9.70	0.021
5.94	0.023	21.7	0.009	23.03	0.016
9.17	0.010	9.37	0.008	14.84	0.006
0.072	**0.092**	**0.090**	**0.121**	**0.355**	**0.263**
		$C_1(t)$			
6.14	0.321	6.09	0.299	6.41	0.223
5.92	0.309	6.49	0.290	1.69	0.221
6.43	0.313	6.85	0.265	1.51	0.141
1.77	0.051	1.61	0.130	7.80	0.140
19.75	0.003	19.80	0.009	9.17	0.111
				9.00	0.068
				7.55	0.048
				19.85	0.013
				22.06	0.010
		$C_2(t)$			
5.42	0.506	5.11	0.573	4.70	0.365
6.45	0.380	6.89	0.335	4.65	0.242
6.80	0.111	7.47	0.086	4.82	0.149
20.02	0.002	20.26	0.005	9.62	0.097
				9.70	0.080
				6.29	0.026
				7.41	0.008

has increased to 0.121. Additional modes with eigenvalues ranging from 4.83 to 21.7 contribute 0.091. The rest (0.021) is contributed by a large number of mixed modes with individual weighting factors below 0.1.

At 45 °C, where $R^c = 0.061$, $c_0^2= 2.42$, and $c_2^2 = -0.74$ was determined for I9γ, only two modes with eigenvalues relatively close to 6 (6.29 and 7.41), with a combined contribution of 0.519, are present. The global motional eigenvalue is close to, but not identical with, the "pure" eigenvalue of $0.366 = 6 \times 0.006$, and the weighting factor of the global motional mode is 0.263. Mixed or coupled (local) modes with eigenvalues ranging from 9.46 to 23.03 contribute 0.218 to $C_0(t)$. Mode-coupling/local motional mode multiplicity is clearly important at 45 °C.

Dynamic modes with eigenvalues relatively close to 6 contribute to $C_1(t)$ ($C_2(t)$) 0.943, 0.854, and 0.411 (0.997, 0.994, and 0.034) at 5, 25 and, 45 °C, respectively. For $C_1(t)$ mode-coupling is significant at 35 °C and dominant at 45 °C. For $C_2(t)$ mode-coupling is very important at 45 °C.

The trends in the various parameters as a function of temperature have been discussed above.

Residual Configurational Entropy. Side-chain $S_{axis}{}^2$ values, which exhibit significantly larger variations than backbone S^2 values, have been used extensively in recent years to calculate residual configurational entropy.[30,52−54] This requires the equilibrium probability distribution function, $P_{eq}(\Omega_{C'M})$, of the M frame relative to the local director, C′. $P_{eq}(\Omega_{C'M})$ is calculated automatically in SRLS using a potential form as general as justified by the quality of the experimental data. The coefficients of this potential, c_0^2 and c_2^2, are determined by fitting the experimental ^{2}H relaxation data. Model-free does not feature potential energy functions (hence equilibrium probability functions) explicitly. Equation 1 features a single order parameter which corresponds to axial potential/axial ordering. Hence one has to adopt a simple form of the potential after fitting, assuming that it is axially symmetric and then use S^2, which is typically inaccurate because of force-fitting, to calculate the coefficient of this (axial) potential. Consequently the residual configurational entropy derived from S^2 is often inaccurate.

Determining the form of the local potential compatible with data integrity and accounting for potential rhombicity are clear advantages of SRLS over MF. Currently the orientation of the spin-bearing bond vectors does not depend explicitly on the other degrees of freedom implying over-estimation of the partition function.[52] Significant improvement on this important aspect is expected to be achieved within the scope of the "integrated approach" discussed below.

Side-Chain Rotamer Interconversion. SRLS is a many-body mode-coupling approach.[24] In principle it can handle any number of local motions coupled to one another and to (asymmetric) global diffusion. The local potential is expanded in the complete basis set of the Wigner rotation matrix elements. The number of terms one may preserve is determined by the nature of the experimental data. We found that the sensitivity of the ^{2}H relaxation data set (including in the current paper rank 2 coherences and relaxation rates acquired at four magnetic fields) does not justify preserving terms beyond the axial and (indispensable) rhombic $L = 2$ components. The local diffusion tensor is axially symmetric, accounting for diffusion *about* and *of* the $C-CH_3$ axis.[23]

This scenario captures many of the major features of methyl dynamics as they emerged from early[55-57] and recent (ref 23 and the current paper) studies. The asymmetry of the local spatial restrictions is represented by the rhombicity of the SRSL potential. The dynamical coupling between the local and global motions (which may occur with arbitrary rates) is intrinsic to the SRLS model. General features of local geometry (e.g., the tilt between the magnetic and local ordering/local diffusion frames) are allowed for automatically in the SRLS formalism. All of the relevant physical quantities can be determined as best-fit parameters.

With regard to rotamer jumps, the SRLS model *can* include potential minima involving motion within the latter, with less frequent jumps between the minima. This is illustrated in Figure 4 of ref 25 and discussed at length in that paper. However, terms of higher rank, L, and order, K, are required to generate such potentials. As pointed out above, data sensitivity does not justify including these terms in the SRLS potential.

Fast rotamer jumps and local librations can be treated separately and combined with SRLS. One of us has used this strategy (using the Stochastic Liouville Equation approach) in the context of ESR of a nitroxide label tethered to a helix mimicking a protein environment.[58,59] In a most general manner, one can combine SRLS with MD simulations, which account for *any* local motion including (relatively fast) rotamer jumps in significantly populated conformations. Moreover, quantum chemical calculations can be used to determine magnetic tensors and hydrodynamic methods to determine the global diffusion tensor.

One of us is currently promoting such an "integrated approach", applied so far to small molecules.[60,61] Our present and recently published[23] SRLS-based methyl dynamics papers constitute an important step toward the application of the "integrated approach" to biomacromolecules. This is currently probably the most advanced attempt to treat methyl dynamics in proteins. The recent study of Hu et al.[39] uses model-free (in particular, the squared generalized order parameter, S^2) combined with molecular mechanics. Unlike SRLS, the MF method does not account for local structural asymmetry, mode-coupling, and general features of local geometry.[21] Only the torsional potential term associated with the C−C bond preceding the $C-CH_3$ axis is considered in ref 39. Conformational multiplicity and additional possible local motions are not accounted for.

Finally, let us point out that methyl dynamics is currently the leading method for studying with NMR mega-Dalton protein systems.[62,63] Therefore efforts to improve the analysis of the experimental data are timely and important.

IV. Conclusions

By applying SRLS to an extensive set of ^{2}H spin relaxation data, we have shown that appropriate analysis of methyl dynamics requires *rhombic* local potentials/local ordering. The model-free $S_{\mathrm{axis}}{}^2$-based "amplitude of motion" picture, implying extensive excursions of the $C-CH_3$ axis in tightly packed protein cores, has been replaced with site-specific potential rhombicity derived with SRLS. The form of the local potential is an important structural property not determined so far with NMR spin relaxation. Potential rhombicity was found to decrease with increasing temperature. The rates for local motions increase on average with increasing temperature. They are approximately 10 times lower than their MF counterparts. Activation energies for methyl motion are estimated at 2 ± 0.2 kcal/mol. These findings are consistent with theoretical predictions derived with molecular dynamics and molecular mechanics methods. The dynamical coupling between the global and the local motions (as estimated by τ/τ_m) increases with increasing temperature. The two-mode approximation is clearly an over simplification, as methyl dynamics is definitely given by the superposition of quite a few modes. The intrinsic ill-definition of the measurable spectral density is reduced considerably using SRLS. The accuracy of the results can be improved by including in the experimental data set rank 2 coherences. Research prospects include elucidation of highly accurate site-specific information, the calculation of residual configurational entropy from experimentally determined rhombic potentials, and enhancements of the dynamic model to include rotamer jumps.

Acknowledgment. This work was supported by the Israel Science Foundation (Grant No. 279/03 to E.M.), the Binational Science Foundation (Grant No. 2000399 to E.M. and J.H.F.), and the Damadian Center for Magnetic Resonance at Bar-Ilan University, Israel. This work was also supported by the National Center for Research Resources of the National Institutes of Health (Grant No. P41-RR016292 to J.H.F.). A.P. acknowledges support of the Italian Ministry for Universities and Scientific and Technological Research projects FIRB and PRIN ex-40%. We thank Prof. Lewis E. Kay of the University of Toronto for providing the experimental data used in this study.

References and Notes

(1) Ishima, R.; Torchia, D. A. *Nat. Struct. Biol.* **2000**, *7*, 740−743.
(2) Case, D. *Acc. Chem. Res.* **2002**, *35*, 325−331.
(3) Bruschweiler, R. *Curr. Opin. Struct. Biol.* **2003**, *13*, 175−183.
(4) Palmer, A. G., III *Chem. Rev.* **2004**, *104*, 3623−3640.
(5) Mittermaier, A.; Kay, L. E. *Science* **2006**, *312*, 224−228.
(6) Igumenova, T. I.; Frederick, K. K.; Wand, A. J. *Chem. Rev.* **2006**, *106*, 1672−1699.
(7) Kitao, A.; Wagner, G. *Mag. Reson. Chem.* **2006**, *44*, S130−S142.
(8) Jarymowycz, V. A.; Stone, M. J. *Chem. Rev.* **2006**, *106*, 1624−1671.
(9) Palmer, A. G.; Massi, F. *Chem. Rev.* **2006**, *106*, 1700−1719.
(10) Muhandiram, D. R.; Yamazaki, T.; Sykes, B. D.; Kay, L. E. *J. Am. Chem. Soc.* **1995**, *117*, 11536−11544.
(11) Millet, O.; Muhandiram, D. R.; Skrynnikov, N. R.; Kay, L. E. *J. Am. Chem. Soc.* **2002**, *124*, 6439−6448.
(12) Srynnikov, N. R.; Millet, O.; Kay, L. E. *J. Am. Chem. Soc.* **2002**, *124*, 6449−6460.
(13) Lipari, G.; Szabo, A. *J. Am. Chem. Soc.* **1982**, *104*, 4546−4559.
(14) Lipari, G.; Szabo, A. *J. Am. Chem. Soc.* **1982**, *104*, 4559−4570.

(15) Clore, G. M.; Szabo, A.; Bax, A.; Kay, L. E.; Driscoll, P. C.; Gronenborn, A. M. *J. Am. Chem. Soc.* **1990**, *112*, 4989−4991.

(16) Tugarinov, V.; Liang, Z.; Shapiro, Y. E.; Freed, J. H.; Meirovitch, E. *J. Am. Chem. Soc.* **2001**, *123*, 3055−3063.

(17) Tugarinov, V.; Shapiro, Y. E.; Liang, Z.; Freed, J. H.; Meirovitch, E. *J. Mol. Biol*. **2002**, *315*, 171−186.

(18) Shapiro, Y. E.; Kahana, E.; Tugarinov, V.; Liang, Z.; Freed, J. H.; Meirovitch, E. *Biochemistry* **2002**, *41*, 6271−6281.

(19) Meirovitch, E.; Shapiro, Y. E.; Tugarinov, V.; Liang, Z.; Freed, J. H. *J. Phys. Chem. B* **2003**, *107*, 9883−9897.

(20) Meirovitch, E.; Shapiro, Y. E.; Liang, Z.; Freed, J. H. *J. Phys. Chem. B* **2003**, *107*, 9898−9904.

(21) Meirovitch, E.; Shapiro, Y. E.; Polimeno, A.; Freed, J. H. *J. Phys. Chem*. A **2006**, *110*, 8366−8396.

(22) Shapiro, Y. E.; Meirovitch, E. *J. Phys. Chem. B 110*, 11519−11524.

(23) Meirovitch, E.; Polimeno, A.; Freed, J. H. *J. Phys. Chem. B* **2006**, *110*, 20615−20628.

(24) Polimeno, A.; Freed, J. H. *Adv. Chem. Phys.* **1993**, *83*, 89−210.

(25) Polimeno, A.; Freed, J. H. *J. Phys. Chem*. **1995**, *99*, 10995−11006.

(26) Liang, Z.; Freed, J. H. *J. Phys. Chem. B* **1999**, *103*, 6384−6396.

(27) (a) Woessner, D. E. *J. Chem. Phys*. **1962**, *36*, 1−4. (b) Chatfield, D. C.; Szabo, A.; Brooks, B. R. *J. Am. Chem. Soc*. **1998**, *120*, 5301−5311. (c) Brainard, J. R.; Szabo, A. *Biochemistry* **1981**, *20*, 4618−4628. (d) Wallach, D. *J. Chem. Phys.* **1967**, *47*, 5258−5268.

(28) Lee, A. L.; Flynn, P. E.; Wand, A. J. *J. Am. Chem. Soc.* **1999**, *121*, 2891−2902.

(29) Lee, A. L.; Sharp, K. A.; Kranz, J. K.; Song, X.-J.; Wand, A. J. *Biochemistry* **2002**, *41*, 13814−13825.

(30) Lee, A. L.; Wand, A. J. *Nature* **2001**, *411*, 501−504.

(31) Prabhu, N. V.; Lee, A. L.; Wand, A. J.; Sharp, K. A. *Biochemistry* **2003**, *42*, 562−570.

(32) Bruschweiler, R.; Wright, P. E. *J. Am. Chem. Soc*. **1994**, *116*, 8426−8427.

(33) Bremi, T.; Bruschweiler, R. *J. Am. Chem. Soc*. **1997**, *119*, 6672−6673.

(34) Lienin, S. F.; Bremi, T.; Brutscher, B.; Bruschweiler, R.; Ernst, R. R. *J. Am. Chem. Soc.* **1998**, *120*, 9870−9879.

(35) Mittermaier, A.; Kay, L. E. *J. Am. Chem. Soc*. **2001**, *123*, 6892−6903.

(36) Chou, J. J.; Case, D. A.; Bax, A. *J. Am. Chem. Soc*. **2003**, *125*, 8959−8966.

(37) Best, R. B.; Clarke, J.; Karplus, M. *J. Am. Chem. Soc*. **2004**, *126*, 7734−7735.

(38) Best, R. B.; Clarke, J.; Karplus, M. *J. Mol. Biol*. **2005**, *349*, 185−203.

(39) Hu, A.; Hermans, J.; Lee, A. L. *J. Biomol. NMR* **2005**, *32*, 151−162.

(40) Freed, H. J.; Nayeem, A.; Rananavare, S. B. In *The Molecular Dynamics of Liquid Crystals*; Luckhurst, G. R., Veracini, C. A., Eds.; Kluwer Academic Publishers: Dordrecht, The Netherlands, 1994; Chapter 12, pp 271−312.

(41) Abragam, A. *Principles of Nuclear Magnetism*; Clarendon Press: Oxford, U.K., 1961.

(42) Peng, J. W.; Wagner, G. In *Nuclear Magnetic Resonance. Part C*; James, T. L., Oppenheimer, N. J., Eds.; Methods in Enzymology, Vol. 239; Academic Press: New York, 1994; pp 563−595.

(43) Tugarinov. V; Kay, L. E. *J. Biomol. NMR* **2004**, *29*, 369−376.

(44) Kay, L. E.; Torchia, D. A.; Bax, A. *Biochemistry* **1989**, *28*, 8972−8979.

(45) Freed, J. H. *J. Chem. Phys.* **1977**, *66*, 4183−4199.

(46) (a) Polimeno, A.; Moro, G. J.; Freed, J. H. *J. Chem. Phys*. **1995**, *104*, 1090−1104. (b) Polnaszek, C. F.; Bruno, G. V.; Freed, J. H. *J. Chem. Phys*. **1973**, *58*, 3185−3199. (c) Polnaszek, C. F.; Freed, J. H. *J. Phys. Chem*. **1975**, *79*, 2283−2306.

(47) Choy, W.-Y.; Kay, L. E. *J. Biomol. NMR* **2003**, *25*, 325−333.

(48) Mandel, A. M.; Akke, M.; Palmer, A. G., III *J. Mol. Biol*. **1995**, *246*, 144−163.

(49) Johnson, E.; Chazin, W. J.; Rance, M. *J. Mol. Biol*. **2006**, *357*, 1237−1252.

(50) Clarkson, M. W.; Gilmore, S. A.; Edgell, M. H.; Lee, A. L. *Biochemistry* **2006**, *45*, 7693−7699.

(51) Chatfield, D. C.; Augusten, A.; D'Cunha, C. *J. Biomol. NMR* **2004**, *29*, 377−385.

(52) Akke, M.; Bruschweiler, R.; Palmer, A. G., III *J. Am. Chem. Soc*. **1993**, *115*, 9832−9833.

(53) Yang, D.; Kay, L. E. *J. Mol. Biol*. **1996**, *263*, 369−382.

(54) Lee, A. L.; Kinnear, S. A.; Wand, A. J. *Nat. Struct. Biol*. **2000**, *7*, 72−77.

(55) Wittebort, R. J.; Szabo, A. *J. Chem. Phys*. **1978**, *69*, 1722−1736.

(56) Avitable, J.; London, R. E. *J. Am. Chem. Soc*. **1978**, *100*, 7159−7165.

(57) Brainard, J. R.; Szabo, A. *Biochemistry* **1981**, *20*, 4618−4628.

(58) Tombolato, F.; Ferrarini, A.; Freed, J. H. *J. Phys. Chem. B* **2006**, *110*, 26248−26259.

(59) Tombolato, F.; Ferrarini, A.; Freed, J. H. *J. Phys. Chem. B* **2006**, *110*, 26260−26271.

(60) Barone, V.; Polimeno, A. *Phys. Chem. Chem. Phys.* **2006**, *8*, 4609−4628.

(61) Barone, V.; Brustolon, M.; Cimino, P.; Polimeno, A.; Zerbetto, M.; Zoleo, A. *J. Am. Chem. Soc.* **2006**, *128*, 15865−25873.

(62) Tugarinov, V.; Sprangers, R.; Kay, L. E. *J. Am. Chem. Soc*. **2007**, *129*, 1743−1750.

(63) Sprangers, R.; Kay, L. E. *Nature* **2007**, *445*, 618−622.